Pergamon

Computers & Fluids Vol. 27, No. 4, pp. 421–433, 1998

Printed in Great Britain
PII: S0045-7930(98)00002-4
0045-7930/98 $19.00 + 0.00

BENCHMARK SPECTRAL RESULTS ON THE LID-DRIVEN CAVITY FLOW

O. BOTELLA[1,2] and R. PEYRET[1,2]*

[1]Laboratoire J.A. Dieudonné, CNRS URM 6621, Université de Nice-Sophia Antipolis, BP 71, 06108 Nice Cedex 2, France
[2]INRIA, BP 93, 06902 Sophia Antipolis Cedex, France

(Received 22 May 1997; in revised form 13 November 1997)

Abstract—Highly-accurate solutions for the lid-driven cavity flow are computed by a Chebyshev collocation method. Accuracy of the solution is achieved by using a substraction method of the leading terms of the asymptotic expansion of the solution of the Navier–Stokes equations in the vicinity of the corners, where the velocity is discontinuous. Critical comparison with former numerical experiments confirms the high-accuracy of the method, and extensive results for the flow at Reynolds number Re = 1000 are presented. © 1998 Elsevier Science Ltd. All rights reserved

1. INTRODUCTION

Since the early work by Burggraf [10], the lid-driven cavity flow is considered as the classical test problem for the assessment of numerical methods and the validation of Navier–Stokes codes. However, the presence of singularities at the two corners where the velocity is discontinuous, makes difficult to properly evaluate the accuracy of the numerical results, mainly in the neighbourhood of these points. This is amplified for spectral Chebyshev methods because their global nature is responsible to extended pollution created by the corner singularities. This is the reason why one may prefer to consider the so-called "regularized driven cavity" (Bourcier and François [7], Peyret and Taylor [19]) where the driving velocity is smoothed so that it vanishes, as well as its derivative, at the corners. In spite of the difficulties above mentioned concerning the singular driven cavity flow and of its physically unrealistic character due to the discontinuous velocity (see, for example, Batchelor [2], Hansen and Kelmanson [15]), the problem is widely used for evaluating incompressible flow solvers. As a result, a large part of the computations concerning this flow are motivated by the validation of a novel method, and do not necessarily pretend to be the most accurate or comprehensive. In contrast, the aim of this paper is to present highly accurate benchmark results for the singular driven cavity flow obtained from a Chebyshev collocation method. For this purpose, a well-established numerical method (Botella [4]) associated with a treatment of the singularities is used, where the accuracy is achieved by calculating a sufficiently smooth solution thanks to the substraction of the leading part of the singularity. The latter is determined from an asymptotic expansion of the solution of the Navier–Stokes equations in the vicinity of the corners, taking the first terms of the expansion into account. Such a technique has already been used in association with Chebyshev methods by Schumack *et al.* [22] for the Stokes equations and by Schultz *et al.* [21] in the case of the Navier–Stokes equations at relatively small values of the Reynolds number. In this last work, only the first singularity of the Stokes problem is removed, so that the calculated solutions remain weakly singular: the pressure and the vorticity gradient behave, respectively, like $\ln r$ and r^{-1}, where r is the distance to the corner. Significant comparisons between the case where the first Stokes singularity only is substracted and the case where the first Navier–Stokes singularity is also removed are made by Botella and Peyret [5].

This substraction method has been applied with success in [5] to the calculation of flows up to the Reynolds number Re = 9000, the latter displaying an unsteady periodic behaviour. Other

*To whom correspondence should be addressed.

steady and unsteady flows, in particular the compressed flow in a piston engine, are computed with the same method in the above reference and in [6]. The results presented in this paper refer essentially to the singular driven cavity flow at Re = 1000. Some results are given for the Stokes flow and the Navier–Stokes flow at Re = 100 for comparison and validation, but our main purpose is to give extensive numerical results in the case Re = 1000, hoping these results could serve as benchmark.

2. PROBLEM FORMULATION AND NUMERICAL SOLUTION

The fluid motion in the driven cavity is governed by the Navier-Stokes equations:

$$\frac{\partial \mathbf{V}}{\partial t} + (\mathbf{V} \cdot \nabla)\mathbf{V} - \frac{1}{\mathrm{Re}} \nabla^2 \mathbf{V} + \nabla \mathbf{p} = 0 \tag{1a}$$

$$\nabla \cdot \mathbf{V} = 0 \tag{1b}$$

to be solved in $\Omega =]0, 1[\times]0, 1[$. In these equations $\mathbf{V} = (u, v)$ is the velocity vector, p is the pressure and Re is the Reynolds number. The associated boundary conditions are $\mathbf{V} = (-1, 0)$ on the side $y = 1$ and $\mathbf{V} = 0$ on the other three sides. The initial condition is either the rest or a calculated solution as it will be explained later.

The well-known difficulty of this problem is the presence of singularities at the corners. At the corners A (0, 1) and B (1, 1), the pressure and the vorticity are not finite, while at the corner C (1, 0) and D (0, 0) the singularity is much weaker since only their second derivatives are unbounded. The effect of the latter on the numerical solution (even spectral) is relatively weak and will not be taken into consideration in the present work. On the other hand, the effect of the singularities at corners A and B cannot be ignored, mainly in the case of a spectral method. The "spectral" accuracy, generally associated to the smoothness of the solution, is then completely lost and the global nature of the approximation induces a pollution phenomenon of the solution.

The effect of the singularities is strongly minimized by substracting the most singular part $(\tilde{\mathbf{V}}, \tilde{p})$ from the solution $(\mathbf{V}, p)$, so that

$$\mathbf{V} = \tilde{\mathbf{V}} + \bar{\mathbf{V}}, \quad p = \tilde{\mathbf{p}} + \bar{\mathbf{p}} \tag{2}$$

with $\tilde{\mathbf{V}} = \mathbf{V}^{\mathrm{A}} + \mathbf{V}^{\mathrm{B}}$ and $\tilde{p} = p^{\mathrm{A}} + p^{\mathrm{B}}$, where $(\mathbf{V}^{\mathrm{s}}, p^{\mathrm{s}})$ refers to the leading terms of the asympotic steady solution near the singular point s = A or s = B. The resulting field $(\bar{\mathbf{V}}, \bar{p})$ is calculated by means of the spectral scheme.

For the determination of $\mathbf{V}^{\mathrm{s}}$ and p^{s} (s = A, B) it is convenient to introduce the steady-state streamfunction ψ (such that $u = \partial\psi/\partial y$, $v = -\partial\psi/\partial x$) and to consider a local coordinate system $x = x_s + r\cos\theta$, $y = y_s + r\sin\theta$, where (x_s, y_s) corresponds to the corner A or B. The equation satisfied by the streamfunction ψ is:

$$-\nabla^4 \psi + \mathrm{Re}\mathbf{V} \cdot \nabla(\nabla^2 \psi) = 0. \tag{3}$$

Now, we are looking for the solution of (3) in the neighbourhood of the singular point (x_s, y_s) as the asymptotic expansion (see Moffatt [18] for the Stokes case):

$$\psi^s = \sum_{k \geq 1} r^{\alpha_k} f_k^s(\theta; \mathrm{Re}) \tag{4}$$

where the exponents α_{k} (which can be complex) are such that

$$1 \leq \mathcal{R}\mathrm{e}(\alpha_1) < \mathcal{R}\mathrm{e}(\alpha_2) < \ldots.$$

These inequalities mean that each term in (4) is less singular than the previous one. This technique of construction does not require the Reynolds number Re to be small.

As a matter of fact, we are interested only in the first two terms in the expansion (4), i.e.

$$\psi^s = r f_1^s(\theta) + r^2 f_2^s(\theta; \mathrm{Re}). \tag{5}$$

The functions f_1^s and $f_2^s = \mathrm{Re}\hat{f}_2^s(\theta)$, already calculated by Inouye [16] and by Gupta *et al.* [14],

are given in Appendix A, along with the corresponding expression of the velocity and pressure. Note that the solution $(\bar{\mathbf{V}}, \bar{p})$ has the following behaviour near the point A:

$$\bar{\mathbf{V}} + \mathbf{V}^{\mathrm{B}} \sim \mathrm{Re}^2 r^2 F_3(\theta), \quad \bar{p} + p^{\mathrm{B}} \sim \mathrm{Re} r G_3(\theta),$$

an analogous behaviour holds near B. It must be recalled [18] that, near the corners C and D, the streamfunction behaves like

$$r^p[\cos(q \ln r) g(\theta) + \sin(q \ln r) h(\theta)]$$

with $p \backsimeq 3.73$, $q \backsimeq 1.12$, g and h being bounded trigonometrical functions.

The quantities $\bar{\mathbf{V}} = (\bar{u}, \bar{v})$ and $\bar{p}$ satisfy to equations similar to Equations (1) with this difference that supplementary terms depending on $\tilde{\mathbf{V}}$ are present. Boundary conditions also depend on $\tilde{\mathbf{V}}$.

3. NUMERICAL SOLUTION AND VALIDATION

The equations for $(\bar{\mathbf{V}}, \bar{p})$ are solved by means of the projection method developed by Botella [3,4] and validated by considering an analytic solution, as well as the flow in the regularized driven cavity. The time-scheme is the second-order accurate version (scheme S21) of the scheme S3 introduced in the above references (see also [5]), where the spatial approximation is based on a strong Chebyshev formulation. In this collocation method, the velocity is approximated with a polynomial of degree N at most in both spatial directions, its values being defined on the $(N+1) \times (N+1)$ Gauss-Lobatto grid

$$\bar{\Omega}_{\mathrm{c}} = \{x_i = (1 - \cos \pi i/N)/2, \quad y_j = (1 - \cos \pi j/N)/2; \quad i, j = 0, \ldots, N\}.$$

On the other hand, the pressure is defined as a polynomial of degree two less, and is calculated at the $(N-1) \times (N-1)$ inner nodes. This $P_N \times P_{N-2}$ discretization prevents the pressure from being polluted by spurious modes, and avoids the necessity to prescribe boundary conditions for the pressure.

The steady-state computed solution is defined by

$$\frac{\max_{\bar{\Omega}_{\mathrm{c}}} | \phi^{n+1} - \phi^n |}{\Delta t \max_{\bar{\Omega}_{\mathrm{c}}} | \phi^{n+1} |} \leq \epsilon \tag{6}$$

where $\phi = \bar{u}, \bar{v}$; Δt is the time step and ϕ^n refers to the numerical approximation at time $n\Delta t$; the value of ϵ will be specified later. We point out that all the results presented hereafter were computed on the DEC AlphaStations 300 5/266 and 3000/2700, using the 64-bit floating point format IEEE $-$ 754 (i.e. giving an accuracy of about 15 digits on real data).

In order to obtain informations on the vortical structure of the cavity flow, we have computed the vorticity $\omega = \partial v/\partial x - \partial u/\partial y$, decomposed as $\omega = \tilde{\omega} + \bar{\omega}$ like in Equation (2), and the streamfunction ψ by solving the Dirichlet problem

$$\nabla^2 \bar{\psi} = -\bar{\omega} \text{ in } \Omega \tag{7a}$$

$$\bar{\psi} = -\tilde{\psi} \text{ on } \partial\Omega, \tag{7b}$$

such that $\psi = \tilde{\psi} + \bar{\psi}$. The singular part $(\tilde{\omega}, \tilde{\psi})$ is given in Appendix A. An alternative way to compute the streamfunction is to solve Equation (7a) with Neumann boundary conditions; however, the comparisons we made on these two determinations of ψ only showed a discrepancy of the order of the accuracy of the overall method (e.g. 2×10^{-6} for the maximum of ψ on $\bar{\Omega}_{\mathrm{c}}$, for $N = 48$ at $\mathrm{Re} = 1000$). In order to take advantage of the global feature of this spectral method, the results on the extrema of the different flow fields displayed in the following tables are obtained by calculating their values on a fine equispaced grid (of mesh size equal to 10^{-4} except when specified), using the analytical formulae for the singular part and Chebyshev polynomial interpolations for the computed part (except for the pressure polynomial $\bar{p}$ which is interpolated using its Lagrangian basis). In a similar fashion, the values of the fields at a given location, which can be found in the various tables, are calculated using polynomial extrapolations and analytical formulae.

Table 1. Some characteristic values of the Stokes flow

Reference	N	Primary vortex	Secondary vortex	$\omega(0, 0.95)$
Present	12	0.10007630	-2.1657×10^{-6}	27.27894
Present	16	0.10007627	-2.2255×10^{-6}	27.27898
Present	24	0.10007627	-2.2279×10^{-6}	27.27903
Present	48	0.10007627	-2.2276×10^{-6}	27.27901
Ref. [21]	29	0.10007	-2.227×10^{-6}	27.2788

Table 2. Extrema of the velocity through the centerlines of the cavity, at Re = 100

Reference	Grid	$u_{\max}$	$y_{\max}$	$v_{\max}$	$x_{\max}$	$v_{\min}$	$x_{\min}$
Present	$N = 16$	0.2139855	0.4581	0.1795006	0.7626	−0.2537294	0.1896
Present	$N = 32$	0.2140423	0.4581	0.1795727	0.7630	−0.2538029	0.1896
Present	$N = 48$	0.2140424	0.4581	0.1795728	0.7630	−0.2538030	0.1896
Present	$N = 64$	0.2140424	0.4581	0.1795728	0.7630	−0.2538030	0.1896
Present	$N = 96$	0.2140424	0.4581	0.1795728	0.7630	−0.2538030	0.1896
Ref. [11]	32×32	0.21064	—	0.17709	—	−0.25179	—
Ref. [11]	44×44	0.21220	—	0.17829	—	−0.25278	—
Ref. [11]	64×64	0.21315	—	0.17896	—	−0.25339	—
Ref. [11]	Extrapolation	0.21405	—	0.17949	—	−0.25399	—
Ref. [12]	129×129	0.21090	0.4531	0.17527	0.7656	−0.24533	0.1953
Ref. [9]	129×129	0.2106	0.4531	0.1786	0.7656	−0.2521	0.1875

First, the accuracy of the method is checked on the Stokes flow defined as the steady solution of Equations (1) where the nonlinear term is discarded and Re = 1. The initial condition is the rest and the steady state is defined by the criterion (6) with $\epsilon = 10^{-10}$. For this flow, the nonlinear singularity $r^2 f_2^s$ in (5) is irrelevant; as a result, due to the linearity of the Stokes equations, the computed solution $(\bar{\mathbf{V}}, \bar{p})$ has a regularity identical to the weakly singular behaviour of the solution at the lower corners C and D. Table 1 shows some characteristic results, more precisely the intensity of the streamfunction at the center of the primary and secondary vortices are given in the third and the fourth columns, while the last column displays the value of the vorticity at point (0, 0.95) close to the upper left corner. These results compare well with those of Schultz *et al*. [21] who used a substraction method of the first Stokes singularity with a streamfunction Chebyshev code. It may be observed that the remaining singularity is weak enough to allow a good convergence of the values of the vorticity near the upper corners.

The second test concerns the flow at Re = 100. Taking the rest as initial condition, the steady-state solution is defined by the criterion (6) with $\epsilon = 10^{-8}$. A first evaluation is made by calculating, as it is usually done for the cavity flow, the velocity extrema along the centerlines of the cavity. The maximum of u on the vertical line $x = 0.5$ is denoted $u_{\max}$ and its location $y_{\max}$. The minimum and maximum of v on the horizontal line $y = 0.5$ are, respectively, denoted $v_{\min}$ and $v_{\max}$; their locations are, respectively, denoted $x_{\min}$ and $x_{\max}$. The values of these extrema, obtained for various values of N, are given in Table 2, along with comparison with previous results found in the literature. These results show that $N = 48$ is sufficient to reach a 7-digit convergence on these extrema. Furthermore, our results are in good agreement with those of Deng *et al*. [11] who performed a Richardson extrapolation of solutions obtained with a finite-volume method.

The convergence of the vorticity is also of interest since this quantity is less regular than the velocity. This field shows a good convergence away from the singularity (see Table 3), but contrary to the Stokes case, the weakly singular nature of the numerical solution in the vicinity of

Table 3. Comparison of the vorticity at the center of the cavity, at Re = 100

	Present	Ref. [17]	
N	$\omega(0.5, 0.5)$	Grid	$\omega(0.5, 0.5)$
16	1.173509		
24	1.174375		
32	1.174410		
48	1.174412	65×65	1.17475
64	1.174412	89×89	1.17442
96	1.174412	Extrapolation	1.17421

Table 4. Convergence of the nonfiltered and filtered vorticity values at the point (0, 0.95) near the upper left corner, at Re = 100

	Present			Ref. [21]	
N	ω, no filter	ω, filter σ_{10}	ω, filter σ_{12}	N	ω
16	−36.61642	−35.87454	−35.88648	11	−25.86
24	−35.88211	−36.09106	−36.09639	14	−31.92
32	−36.13314	−36.08042	−36.08073	17	−36.56
48	−36.08094	−36.07734	−36.07715	20	−37.40
64	−36.07343	−36.07637	−36.07629	23	−35.64
96	−36.07535	−36.07635	−36.07635	29	−35.64

Table 5. Convergence of the nonfiltered and filtered vorticity values at the point (0.5, 1) on the moving wall, at Re = 100

	Present			Ref. [17]	
N	ω, no filter	ω, filter σ_{10}	ω, filter σ_{12}	Grid	ω
16	6.587295	6.563304	6.564057		
24	6.567463	6.563380	6.564017		
32	6.564784	6.564035	6.564089		
48	6.564161	6.564093	6.564094	65×65	6.5606
64	6.564107	6.564094	6.564094	89×89	6.5626
96	6.564091	6.564094	6.564094	Extrapolation	6.5638

the upper corners (the vorticity behaves like $\mathrm{Re}^2 r H_3(\theta)$) slows down its convergence. This is illustrated in Table 4 where the values of the vorticity at location (0, 0.95) with respect to N are compared with those of Schultz *et al.* [21].

A filtering postprocessing has been considered in order to improve the accuracy of the vorticity along the boundaries. This can be obtained by applying to the Chebyshev spectrum of the computed vorticity $\bar{\omega}$ the filters σ_q introduced by Vandeven [23], where q denotes the order of the filter. The efficiency of this filtering postprocessing with respect to q is discussed in Section 4 for the Re = 1000 case (see also [5]). However, in order to make a preliminary evaluation of this postprocessing, some results are given for the Re = 100 case by considering two points for which comparative results are available: one is located at (0.5, 1) far from the singularity and for which we have the results of Luchini [17], and the other one is the point (0, 0.95), close to the upper left corner, already considered in [21]. Table 5 compares the values of the filtered (with $q = 10$ or 12) and nonfiltered vorticity at location $x = 0.5$ on the moving wall and the extrapolated results obtained in [17] using a third-order conservative finite-difference scheme. At location (0, 0.95) near the singularity, the enhanced accuracy of the filtered vorticity is made clear in Table 4: a 7-digit convergence is found using the σ_{10} and σ_{12} filters, while the nonfiltered field only reached a 4-digit accuracy for $N = 96$. As far as the raw results are concerned, the favorable effect of the substraction of the first two singular terms is clearly shown when comparing the present nonfiltered results with those obtained in [21].

Extensive results for Re = 1000 are given in Section 4. However, some results are presented here for the sake of validation. The steady solutions, characterized by $\epsilon = 10^{-10}$, were computed

Table 6. Intensities of the primary vortex, at Re = 1000; (x, y) refers to the center of the primary vortex, i.e. the location of the maximum value of the streamfunction

Reference	Grid	ψ	ω	x	y
Present	$N = 48$	0.1189249	2.067396	0.4692	0.5652
Present	$N = 64$	0.1189365	2.068016	0.4692	0.5652
Present	$N = 96$	0.1189366	2.067750	0.4692	0.5652
Present	$N = 128$	0.1189366	2.067750	0.4692	0.5652
Present	$N = 160$	0.1189366	2.067753	0.4692	0.5652
Ref. [1]	257×257	0.118930	—	—	—
Ref. [20]	100×100	0.11315	1.9863	—	—
Ref. [20]	121×121	0.11492	2.0112	—	—
Ref. [20]	141×141	0.11603	2.0268	0.47143	0.56429
Ref. [20]	Extrapolation	0.11894	2.0677	—	—
Ref. [12]	129×129	0.117929	2.04968	0.4687	0.5625
Ref. [9]	256×256	0.1163	—	0.4687	0.5586
Ref. [13]	129×129	0.1157	—	0.4688	0.5625
Ref. [24]	321×321	0.1173	—	0.4562	0.5625

Table 7. The value and the corresponding label of the streamfunction contours displayed in Fig. 1. Note that for the sake of clarity of the figure some of the contours are not labelled

Streamfunction						
Value	0.1175	0.115	0.11	0.1	9×10^{-2}	7×10^{-2}
label	a		b		c	
Value	5×10^{-2}	3×10^{-2}	$1x10^{-2}$	1×10^{-4}	1×10^{-5}	1×10^{-10}
label	d		e	f		
Value	0.0	-1×10^{-6}	-1×10^{-5}	-5×10^{-5}	-1×10^{-4}	-2.5×10^{-4}
label			g		h	
Value	-5×10^{-4}	-1×10^{-3}	-1.5×10^{-3}			
label	i		j			

Table 8. The value and the corresponding label of the vorticity and pressure contours displayed in Figs 2 and 3, respectively

Vorticity											
Value	5.0	4.0	3.0	2.0	1.0	0.5	0.0	−0.5	−1.0	−2.0	−3.0
label	a	b	c	d	e	f	g	h	i	j	k
Pressure											
Value	0.3	0.17	0.12	0.11	0.09	0.07	0.05	0.02	0.0	−0.002	
label	a	b	c	d	e	f	g	h	i	j	

using various grids defined by the polynomial degree $N = 48$, 64, 96, 128 and 160. The initial condition is defined as the solution obtained with a code where only the first Stokes singularity is substracted. Results for the values of the streamfunction and the vorticity calculated at the center of the primary vortex are given in Table 6. These results show the perfect convergence with respect to N of the considered quantities. Their accuracy is made clear when compared to the results of Schreiber and Keller [20], who performed a Richardson extrapolation (theoretically of sixth-order in space) using finite-difference solutions obtained on 100×100, 121×121 and 141×141 grids. Good agreement is also found with the results of Barragy and Carey [1] on the maximum of ψ, computed using a p finite element method. It may be concluded that the 97×97 grid Chebyshev solution is sufficient to obtain at least an accuracy comparable to the one shown in the above two references.

We have to mention that the high accuracy which should be attained when using a spectral method with a large number of N, such as $N = 160$, may be affected by round-off errors. This matter concerns in particular the vorticity field, which is the most sensitive quantity since it is obtained from differentiation of primitive variables. For all the results gathered in the case $\mathrm{Re} = 1000$, it seems that the seventh digit of the vorticity for $N = 160$ is questionable, as it can be seen in the fourth column of Table 6. Concerning the other fields, the results addressed in the following section seem unalduterated by round-off errors, except the low intensities of the tertiary vortices given in Table 14 and Table 15.

Table 9. Horizontal velocity, pressure and vorticity through the vertical centerline of the cavity at $\mathrm{Re} = 1000$, computed at the locations given in [12], using the $N = 160$ solution

y	u, Ref. [12]	u	p	ω
1.0000	−1.00000	−1.0000000	0.052987	14.7534
0.9766	−0.65928	−0.6644227	0.052009	12.0670
0.9688	−0.57492	−0.5808359	0.051514	9.49496
0.9609	−0.51117	−0.5169277	0.050949	6.95968
0.9531	−0.46604	−0.4723329	0.050329	4.85754
0.8516	−0.33304	−0.3372212	0.034910	1.76200
0.7344	−0.18719	−0.1886747	0.012122	2.09121
0.6172	−0.05702	−0.0570178	−0.000827	2.06539
0.5000	0.06080	0.0620561	0.000000	2.06722
0.4531	0.10648	0.1081999	0.004434	2.06215
0.2813	0.27805	0.2803696	0.040377	2.26772
0.1719	0.38289	0.3885691	0.081925	1.05467
0.1016	0.29730	0.3004561	0.104187	−1.63436
0.0703	0.22220	0.2228955	0.108566	−2.20175
0.0625	0.20196	0.2023300	0.109200	−2.31786
0.0547	0.18109	0.1812881	0.109689	−2.44960
0.0000	0.00000	0.0000000	0.110591	−4.16648

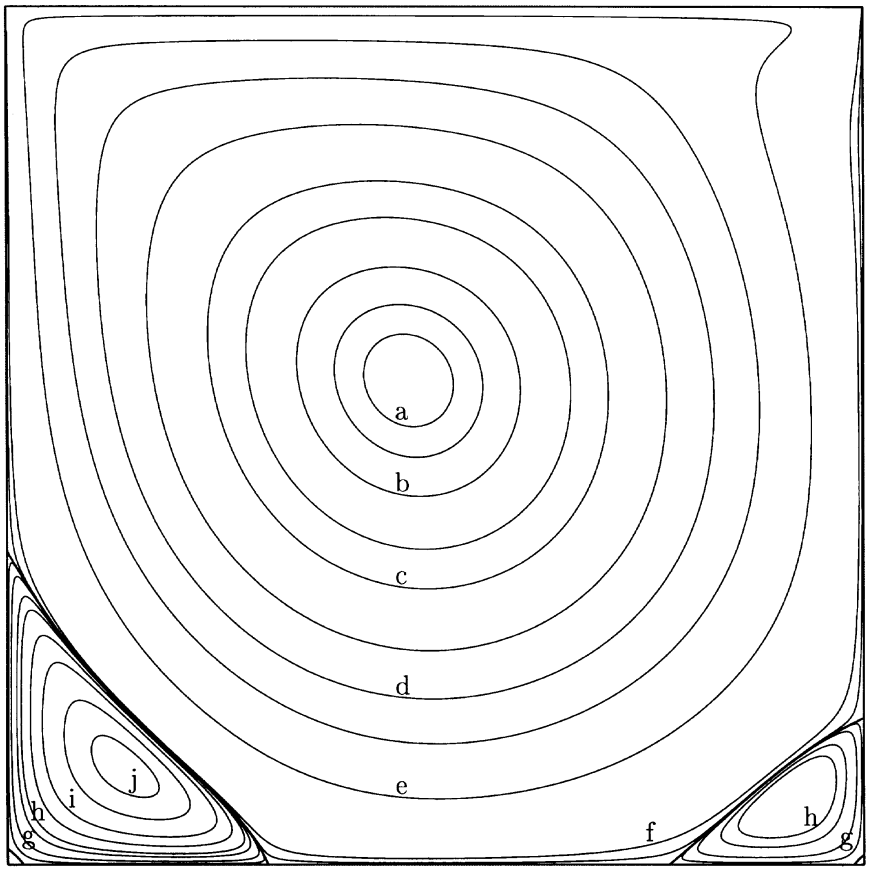

Fig. 1. Streamlines of the flow at Re = 1000, using the $N = 128$ solution.

4. BENCHMARK RESULTS FOR THE FLOW AT RE = 1000

Comprehensive results on the flow at Re = 1000 are displayed in Table 7 and following. The results on the pressure fields are given after setting the pressure equal to zero at the center (0.5, 0.5) of the cavity. Isovalues of the streamfunction, vorticity and pressure fields are, respectively, displayed on Fig. 1, Fig. 2 and Fig. 3, using the $N = 128$ solution interpolated on a 513×513 Chebyshev-Gauss-Lobatto grid. At the scale of the figures, the iso-contour lines corresponding to the $N = 160$ solution are indistinguishable from the presented ones. The streamfunction contour values and the labels are given in Table 7. Iso-vorticity and isobaric contour values (and their corresponding label) are given in Table 8.

Table 10. Vertical velocity, pressure and vorticity through the horizontal centerline of the cavity at Re = 1000, computed at the locations given in [12], using the $N = 160$ solution

x	v, Ref. [12]	v	p	ω
0.0000	0.00000	0.0000000	0.077455	−5.46217
0.0312	−0.21388	−0.2279225	0.078837	−8.44350
0.0391	−0.27669	−0.2936869	0.078685	−8.24616
0.0469	−0.33714	−0.3553213	0.078148	−7.58524
0.0547	−0.39188	−0.4103754	0.077154	−6.50867
0.0937	−0.51550	−0.5264392	0.065816	0.92291
0.1406	−0.42665	−0.4264545	0.049029	3.43016
0.1953	−0.31966	−0.3202137	0.034552	2.21171
0.5000	0.02526	0.0257995	0.000000	2.06722
0.7656	0.32235	0.3253592	0.044848	2.06122
0.7734	0.33075	0.3339924	0.047260	2.00174
0.8437	0.37095	0.3769189	0.069511	0.74207
0.9062	0.32627	0.3330442	0.084386	−0.82398
0.9219	0.30353	0.3099097	0.086716	−1.23991
0.9297	0.29012	0.2962703	0.087653	−1.50306
0.9375	0.27485	0.2807056	0.088445	−1.83308
1.0000	0.00000	0.0000000	0.090477	−7.66369

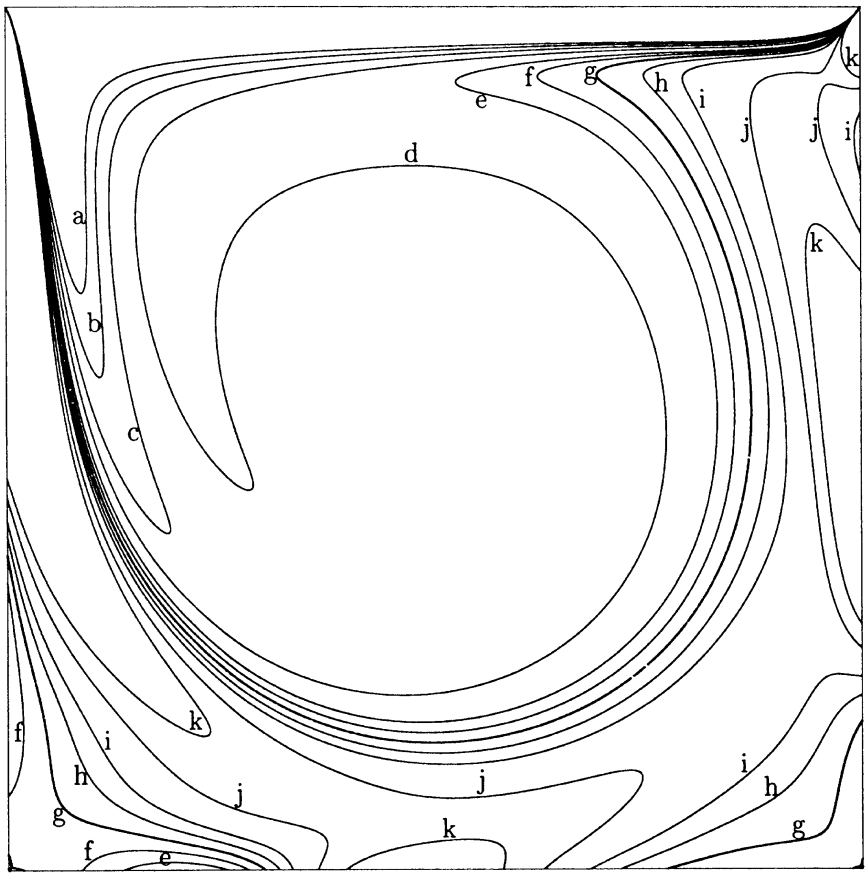

Fig. 2. Iso-vorticity lines of the flow at Re = 1000, using the $N = 128$ solution.

An update of the data on the velocity profiles given in the early paper by Ghia *et al.* [12], which is the most referred source of results on the driven cavity flow, is displayed in Table 9 and Table 10 using the $N = 160$ solution. The values of the pressure and the vorticity at the same points are also presented in these tables. We point out that the differences between these results and those obtained for $N = 128$ are at most 10^{-6} for u, v and p, and 6×10^{-5} for ω. The values of the extrema of the velocity through the centerline of the cavity, obtained for the various values of N, are given in Table 11 and compared with those found in the literature. As for the Re = 100 case, good agreement is found with the extrapolated results of Deng *et al.* [11], obtained with two distinct finite-volume methods.

Table 11. Extrema of the velocity through the centerlines of the cavity, at Re = 1000

Reference	Grid	u_{max}	y_{max}	v_{max}	x_{max}	v_{min}	x_{min}
Present	$N = 48$	0.3885271	0.1717	0.3768991	0.8422	−0.5270168	0.0908
Present	$N = 64$	0.3885695	0.1717	0.3769439	0.8422	−0.5270763	0.0908
Present	$N = 96$	0.3885698	0.1717	0.3769447	0.8422	−0.5270771	0.0908
Present	$N = 128$	0.3885698	0.1717	0.3769447	0.8422	−0.5270771	0.0908
Present	$N = 160$	0.3885698	0.1717	0.3769447	0.8422	−0.5270771	0.0908
Ref. [11], cpi	64×64	0.37436	—	0.36364	—	−0.51015	—
Ref. [11], cpi	96×96	0.38233	—	0.37109	—	−0.51947	—
Ref. [11], cpi	128×128	0.38511	—	0.37369	—	−0.52280	—
Ref. [11], cpi	Extrapolation	0.38867	—	0.37702	—	−0.52724	—
Ref. [11], stagg.	64×64	0.375726	—	0.34556	—	−0.48858	—
Ref. [11], stagg.	96×96	0.37441	—	0.36271	—	−0.50982	—
Ref. [11], stagg.	128×128	0.38050	—	0.36884	—	−0.51727	—
Ref. [11], stagg.	Extrapol.	0.38855	—	0.37705	—	−0.52690	—
Ref. [12]	129×129	0.38289	0.1719	0.37095	0.8437	−0.51550	0.0937
Ref. [9]	256×256	0.3764	0.1602	0.3665	0.8477	−0.5208	0.0898
Ref. [24]	321×321	0.387	0.1734	—	—	—	—

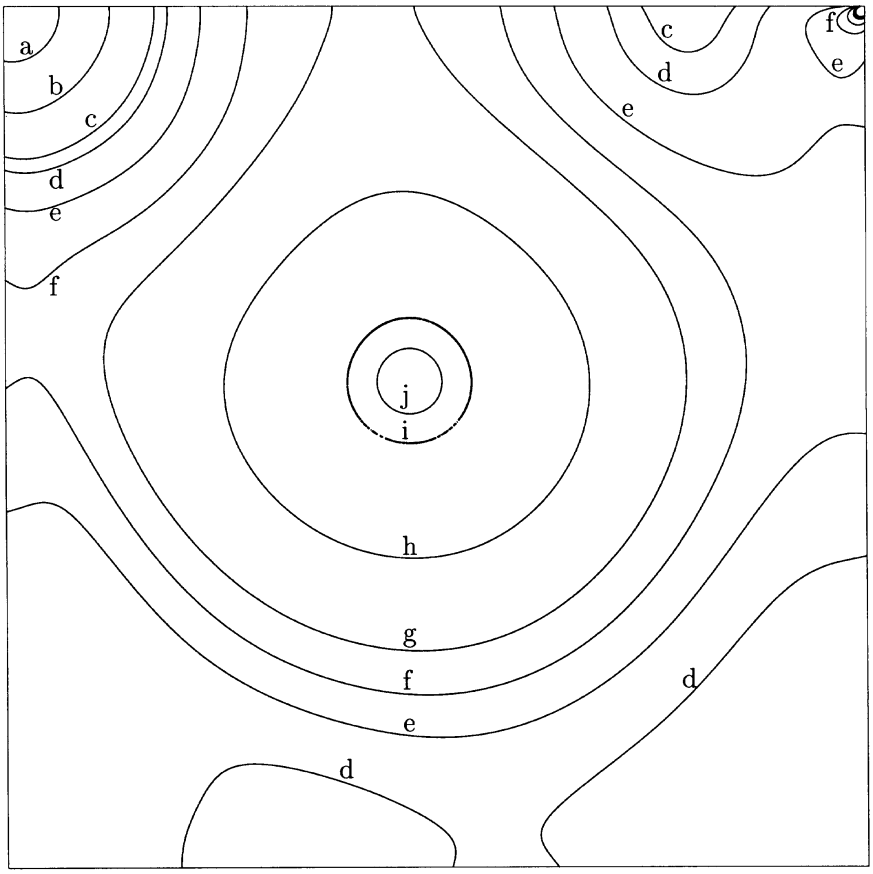

Fig. 3. Isobaric lines of the flow at Re = 1000, using the $N = 128$ solution.

Table 12 through Table 15 show the intensities of the secondary and tertiary vortices obtained with the various values of N; comparison with the literature is also given. Due to the minute size of the latter vortices, their location is given with an error $\pm 10^{-5}$. To be complete, we recall that the results on the primary vortex are displayed in Table 6. It may be noticed that the tertiary vortices appear in the Chebyshev solution with the relatively coarse grid 65×65 thanks to the dense distribution of the collocation points near the corners.

All the results already displayed exhibit a very good convergence, with respect to N, throughout the domain except in the near vicinity of the upper corners. For a further illustration of such a behaviour, the values of the pressure at points (0.1, 0.1) and (0.8, 0.5) are given in the second and third columns of Table 16. At point (0, 0.95), which is close to the upper left corner, the convergence of the pressure is relatively good, as shown in the fourth column of Table 16. On the other hand, at the same point, the convergence of the vorticity is not so clear when observing the second column of Table 17.

Table 12. Intensities of the lower left secondary vortex, at Re = 1000; (x, y) gives the location of the value of the streamfunction minimum

Reference	ψ	ω	x	y
Present, $N = 48$	-1.728963×10^{-3}	-1.109440	0.1360	0.1118
Present, $N = 64$	-1.729687×10^{-3}	-1.109714	0.1360	0.1118
Present, $N = 96$	-1.729716×10^{-3}	-1.109772	0.1360	0.1118
Present, $N = 128$	-1.729717×10^{-3}	-1.109794	0.1360	0.1118
Present, $N = 160$	-1.729717×10^{-3}	-1.109789	0.1360	0.1118
Ref. [12]	-1.75102×10^{-3}	-1.15465	0.1406	0.1094
Ref. [9]	-1.91×10^{-3}	—	0.1289	0.1094
Ref. [20]	-1.700×10^{-3}	-0.9990	0.13571	0.10714
Ref. [13]	-1.63×10^{-3}	—	0.1329	0.1171
Ref. [24]	-1.74×10^{-3}	—	0.1375	0.1063

Table 13. Intensities of the lower right secondary vortex, at Re = 1000; (x, y) gives the location of the value of the streamfunction minimum

Reference	ψ	ω	x	y
Present, $N = 48$	-2.333584×10^{-4}	−0.3516751	0.9167	0.0781
Present, $N = 64$	-2.334531×10^{-4}	−0.3521015	0.9167	0.0781
Present, $N = 96$	-2.334529×10^{-4}	−0.3522603	0.9167	0.0781
Present, $N = 128$	-2.334528×10^{-4}	−0.3522832	0.9167	0.0781
Present, $N = 160$	-2.334528×10^{-4}	−0.3522861	0.9167	0.0781
Ref. [12]	-2.31129×10^{-4}	−0.36175	0.9141	0.0781
Ref. [9]	-3.25×10^{-4}	—	0.9141	0.0820
Ref. [20]	-2.1700×10^{-4}	−0.30200	0.91429	0.07143
Ref. [13]	-2.11×10^{-4}	—	0.9141	0.0781
Ref. [24]	-2.24×10^{-4}	—	0.9250	0.0813

Table 14. Intensities of the lower left tertiary vortex, at Re = 1000; (x, y) gives the location of the value of the streamfunction maximum

Reference	ψ	x	y
Present, $N = 64$	5.88479×10^{-8}	0.00741	0.00799
Present, $N = 96$	5.01978×10^{-8}	0.00774	0.00753
Present, $N = 128$	5.03992×10^{-8}	0.00768	0.00765
Present, $N = 160$	5.03944×10^{-8}	0.00768	0.00765
Ref. [12]	9.31929×10^{-8}	0.0078	0.0078
Ref. [13]	8.79×10^{-8}	0.0079	0.0078

For the pressure and vorticity values close to the upper corners, the convergence with respect to N can be improved by using the filters σ_q as mentioned in the previous section and already applied to the Re = 100 case. However, care must be taken when using these filters for recovering accuracy near singular points. The order q of these filters is a deceptive notion: it is known (Vandeven [23], Boyd [8]) that the application of the Vandeven filter σ_q does not yield a pointwise error of order q uniformly in space but rather, as the distance to the singular point decreases, the order of accuracy falls until reaching an O(1) error very close to the singularity. Furthermore, a high-order filter is expected to give worse results than a low order one (or no filter at all) near the singular point. As a result, the optimal choice of q for recovering accuracy depends on its nearness to the singular point (see [8]). In order to evaluate the limit of the filtering postprocessing, filters of various orders are applied to the vorticity $\bar{\omega}$ at a sequence of points located at a decreasing distance to the singular upper left corner. First, Table 17 displays the convergence of the vorticity at point (0, 0.95) with respect to N, obtained without filtering and with the application of the filters σ_q, with $q = 2$, 6, 10, 12 and 18. Up to this distance at least, high-order filtering is effective: a 7-digit convergence is found on the values obtained with the last three filters, while the lower-order filtering with $q = 2$ or 6 proves to be insufficient.

Table 15. Intensities of the lower right tertiary vortex, at Re = 1000; (x, y) gives the location of the value of the streamfunction maximum

Reference	ψ	x	y
Present, $N = 64$	2.08635×10^{-8}	0.99642	0.00452
Present, $N = 96$	6.45556×10^{-9}	0.99513	0.00424
Present, $N = 128$	6.33255×10^{-9}	0.99510	0.00482
Present, $N = 160$	6.39800×10^{-9}	0.99516	0.00484
Ref. [9]	3.06×10^{-9}	0.9961	0.0039

Table 16. Convergence of the pressure at various points, at Re = 1000. The second and third columns correspond to points away from the upper corners, the last three give nonfiltered and filtered values of the pressure at point (0, 0.95) close to the upper left corner

N	(0.1, 0.1) p, no filter	(0.8, 0.5) p, no filter	(0, 0.95) p, no filter	p, filter σ_{10}	p, filter σ_{12}
48	0.1067136	0.055736	0.3561904	0.3568328	0.3570182
64	0.1067350	0.055743	0.3556856	0.3553249	0.3553056
96	0.1067353	0.055743	0.3551954	0.3552370	0.3552367
128	0.1067353	0.055743	0.3552255	0.3552370	0.3552370
160	0.1067353	0.055743	0.3552442	0.3552369	0.3552369

Table 17. Convergence of the vorticity and its filtered counterpart at the location (0, 0.95) near the upper left corner at Re = 1000

N	ω, no filter	ω, filter σ_2	ω, filter σ_6	ω, filter σ_{10}	ω, filter σ_{12}	ω, filter σ_{18}
48	−84.24558	−83.88683	−83.80277	−83.82890	−83.86083	−83.97431
64	−83.47874	−83.88016	−83.81269	−83.82606	−83.82833	−83.81381
96	−83.70878	−83.84503	−83.81859	−83.82052	−83.82041	−83.82069
128	−83.88577	−83.83416	−83.82000	−83.82036	−83.82035	−83.81988
160	−83.82351	−83.82935	−83.82026	−83.82035	−83.82035	−83.82035

Table 18. Convergence of the vorticity and its filtered counterpart at the location (0, 0.999) near the upper left corner, at Re = 1000

N	ω, no filter	ω, filter σ_2	ω, filter σ_4	ω, filter σ_6	ω, filter σ_{12}
48	−1431.335	−1438.750	−1438.659	−1438.443	−1438.139
64	−1438.343	−1442.290	−1442.204	−1442.096	−1441.994
96	−1445.406	−1444.428	−1444.325	−1444.317	−1444.370
128	−1445.489	−1444.865	−1444.801	−1444.807	−1444.838
160	−1444.611	−1444.891	−1444.885	−1444.898	−1444.911

Furthermore, at this location the orders $q = 10$ or 12 are not far from being optimal. One may observe that good agreement is found with the predicted optimal order given in [8] which is e.g. $q_{\text{opt}} \backsimeq 10.1$ for $N = 128$ and $q_{\text{opt}} \backsimeq 12.4$ for $N = 160$. Then the point (0, 0.999), located much closer to the singularity than the previous one, is considered. The vorticity values obtained without filtering and with the filters σ_2, σ_4, σ_6 and σ_{12} are reported in Table 18. At this location, filtering is still valid, although at this distance the low-order filters σ_2 and σ_4 seem preferable to the σ_{12} filter. Note that the corresponding optimal order is given as $q_{\text{opt}} \backsimeq 2.3$ for $N = 128$ and $q_{\text{opt}} \backsimeq 4.2$ for $N = 160$. Finally, when the distance to the singular point is very small, the filtering of $\bar{\omega}$ is not only inefficient but also give bad results, as it has been observed at point (0, 0.99999). However, note that when the distance to the singular corner is sufficiently small, the leading part of the asymptotic expansion of the solution is largely predominant over the computed solution. More precisely, at the point (0, 0.99999), the singular part is $\tilde{\omega} \simeq 1.3 \times 10^5$ while the computed solution is $\bar{\omega} \backsimeq -61$. As a result, the filtering of $\bar{\omega}$ does not change significantly the complete solution and is, in fact, useless.

Taking this discussion into account, the filtered pressure results at the point (0, 0.95) obtained with the filters σ_{10} and σ_{12} are given in the last two columns of Table 16. They show a behaviour similar to the one encountered for the vorticity at the same point.

At last, the values of the vorticity along the moving wall $y = 1$, at locations already considered by Ghia *et al.* [12], are given in Table 19. At these locations, the difference between the filtered values (using the σ_{10} or σ_{12} filter) obtained for $N = 128$ and $N = 160$ is found to be less than 4×10^{-6}. Up to the number of digits given in the last column of Table 19, the filtered $N = 128$ and $N = 160$ solutions are identical. On the other hand, when compared with the filtered results, the $N = 128$ solution shows a maximum difference of 10^{-2} while this difference

Table 19. Vorticity values on the moving wall ($y = 1$) at Re = 1000, computed with the $N = 160$ solution at the locations given in [12]

x	ω, Ref. [12]	ω, no filter	ω, filter σ_{12}
1.0000	—	—	—
0.9375	75.5980	72.63317	72.63795
0.8750	51.0557	50.50948	50.50730
0.8125	40.5437	40.21154	40.21384
0.7500	32.2953	32.01094	32.01224
0.6875	25.4341	25.19322	25.19252
0.6250	20.2666	20.06664	20.06667
0.5625	16.8350	16.67047	16.66992
0.5000	14.8901	14.75344	14.75342
0.4375	14.0928	13.97977	13.98148
0.3750	14.1374	14.05230	14.05334
0.3125	14.8061	14.75553	14.75229
0.2500	16.0458	16.02546	16.02919
0.1875	18.3120	18.35148	18.35666
0.1250	23.8707	24.06088	24.05671
0.0625	42.1124	42.69943	42.70770
0.0000	—	—	—

reduces to 5×10^{-3} for the $N = 160$ solution. Finally, taking as reference the filtered results, it must be noticed that the maximum error found for $N = 128$ is lower than 0.02% while it is 4% at most for the finite-difference results of Ghia *et al.* [12]. This illustrates the gain in accuracy which can be obtained, particularly in the vicinity of the upper corners, when the numerical method associates high-order spectral approximation and a suitable treatment of the corner singularities.

REFERENCES

1. Barragy, E. and Carey, G. F., Stream function-vorticity driven cavity solution using p finite elements, *Computers and Fluids*, 1997, **26,** 453–468.
2. Batchelor, G. K., An Introduction to Fluid Dynamics. Cambridge University Press, 1967.
3. Botella, O., *Résolution des équations de Navier–Stokes par des schémas de projection Tchebychev*, INRIA research report, No. 3018, 1996.
4. Botella, O., On the solution of the Navier–Stokes equations using Chebyshev projection schemes with third-order accuracy in time, *Computers and Fluids*, 1997, **26,** 107–116.
5. Botella, O. and Peyret, R., Computing singular solutions of the Navier–Stokes equations with the Chebyshev collocation method, to be published.
6. Botella, O. and Peyret, R., The Chebyshev approximation for the solution of singular Navier–Stokes problems. To be published in, *Proceedings of the Third Summer Conference on Numerical Modelling in Continuum Mechanics*, Prague, September 8–11, 1997.
7. Bourcier, M. and François, C., Intégration numérique des équations de Navier–Stokes dans un domaine carré, *La Recherche Aérospatiale*, 1969, No. 131, 23–33.
8. Boyd, J. P., The Erfc-Log filter and the asymptotics of the Euler and Vandeven sum accelerations. In *Proceedings of the Third International Conference on Spectral and High Order Methods*, ed. A. V. Ilin and L. R. Scott. Houston Journal of Mathematics, Houston, Texas, 1996, pp. 267–276.
9. Bruneau, C-H. and Jouron, C., An efficient scheme for solving steady incompressible Navier–Stokes equations, *Journal of Computational Physics*, 1990, **89,** 389–413.
10. Burggraf, O. R., Analytical and numerical studies of the structure of steady separated flows, *Journal of Fluid Mechanics*, 1966, **24,** 113–151.
11. Deng, G. B., Piquet, J., Queutey, P. and Visonneau, M., Incompressible flow calculations with a consistent physical interpolation finite volume approach, *Computers and Fluids*, 1994, **23,** 1029–1047.
12. Ghia, U., Ghia, K. N. and Shin, C. T., High-Re solutions for incompressible flow using the Navier–Stokes equations and a multigrid method, *Journal of Computational Physics*, 1982, **48,** 387–411.
13. Goyon, O., High-Reynolds number solutions of Navier–Stokes equations using incremental unknowns, *Computer Methods in Applied Mechanics and Engineering*, 1996, **130,** 319–335.
14. Gupta, M. M., Manohar, R. P. and Noble, B., Nature of viscous flows near sharp corners, *Computers and Fluids*, 1981, **9,** 379–388.
15. Hansen, E. B. and Kelmanson, M. A., An integral equation justification of the boundary conditions of the driven cavity problem, *Computers and Fluids*, 1994, **26,** 225–240.
16. Inouye, K., Ecoulement d'un fluide visqueux dans un angle droit, *Journal de Mécanique*, 1973, **12,** 609–628.
17. Luchini, P., Higher-order difference approximations of the Navier–Stokes equations, *International Journal on Numerical Methods in Fluids*, 1991, **12,** 491–506.
18. Moffatt, H. K., Viscous and resistive eddies near a sharp corner, *Journal of Fluid Mechanics*, 1964, **18,** 1–18.
19. Peyret, R. and Taylor, T. D., *Computational Methods for Fluid Flow*, Springer, New York, 1983.
20. Schreiber, R. and Keller, H. B., Driven cavity flows by efficient numerical techniques, *Journal of Computational Physics*, 1983, **49,** 310–333.
21. Schultz, W. W., Lee, N. Y. and Boyd, J. P., Chebyshev pseudospectral method of viscous flows with corner singularities, *Journal of Scientific Computing*, 1989, **4,** 1–24.
22. Schumack, M. R., Schultz, W. W. and Boyd, J. P., Spectral method solution of the Stokes equations on nonstaggered grids, *Journal of Computational Physics*, 1991, **94,** 30–58.
23. Vandeven, H., Family of spectral filters for discontinuous problems, *Journal of Scientific Computing*, 1991, **6,** 159–192.
24. Vanka, S. P., Block-implicit multigrid solution of Navier–Stokes equations in primitive variables, *Journal of Computational Physics*, 1986, **65,** 138–158.

5. APPENDIX A

Expression of the Singular Part ($\tilde{\mathbf{V}}$, $\tilde{p}$)

The singular part $\tilde{\mathbf{V}} = \mathbf{V}^{\mathrm{A}} + \mathbf{V}^{\mathrm{B}}$ and $\tilde{p} = p^{\mathrm{A}} + p^{\mathrm{B}}$ is calculated from ψ^s, (s = A, B), defined by Equation (5). At corner A (0, 1), the polar coordinates are defined by $x = r \cos\theta$, $y = 1 + r \sin\theta$, with $\theta \in [-\pi/2, 0]$, and ψ^{A} has the following expression (Inouye [16], Gupta *et al.* [14]):

$$\Psi^{\mathrm{A}} = r f_1^{\mathrm{A}}(\theta) + r^2 f_2^{\mathrm{A}}(\theta; \mathrm{Re})$$

with

$$f_1^{\mathrm{A}}(\theta) = \frac{1}{\alpha}\left(\theta\cos\theta - \left(\frac{\pi^2}{4} + \frac{\pi}{2}\theta\right)\sin\theta\right)$$

$$f_2^{\mathrm{A}}(\theta; \mathrm{Re}) = \mathrm{Re}(\mathrm{A}_0 + \mathrm{A}_1\theta + (-\mathrm{A}_0 + \mathrm{B}_1\theta + \mathrm{B}_2\theta^2)\cos 2\theta + (\mathrm{C}_0 + \mathrm{C}_1\theta + \mathrm{C}_2\theta^2)\sin 2\theta).$$

The velocity, pressure and vorticity have the following expression:

$$u^{\mathrm{A}} = u_1^{\mathrm{A}}(\theta) + r u_2^{\mathrm{A}}(\theta; \mathrm{Re}), \quad v^{\mathrm{A}} = v_1^{\mathrm{A}}(\theta) + r v_2^{\mathrm{A}}(\theta; \mathrm{Re})$$

$$p^{\mathrm{A}} = r^{-1} p_1^{\mathrm{A}}(\theta; \mathrm{Re}) + p_2^{\mathrm{A}} \ln r, \quad \omega^{\mathrm{A}} = r^{-1}\omega_1^{\mathrm{A}}(\theta) + \omega_2^{\mathrm{A}}(\theta; \mathrm{Re})$$

with

$$u_1^{\mathrm{A}}(\theta) = \frac{1}{\alpha}\left(\frac{1}{2} - \frac{\pi^2}{4} - \frac{\pi}{2}\theta + \frac{1}{2}\cos 2\theta - \frac{\pi}{4}\sin 2\theta\right)$$

$$v_1^{\mathrm{A}}(\theta) = \frac{1}{\alpha}\left(-\theta - \frac{\pi}{4} + \frac{1}{2}\sin 2\theta + \frac{\pi}{4}\cos 2\theta\right)$$

$$p_1^{\mathrm{A}}(\theta; \mathrm{Re}) = \frac{1}{\alpha \mathrm{Re}}(2\cos\theta - \pi\sin\theta)$$

$$\omega_1^{\mathrm{A}}(\theta) = \frac{1}{\alpha}(\pi\cos\theta + 2\sin\theta)$$

and

$$u_2^{\mathrm{A}}(\theta; \mathrm{Re}) = \mathrm{Re}\left\{\left(2\mathrm{C}_2\theta^2 + (2\mathrm{C}_1 + \mathrm{B}_2)\theta + \mathrm{A}_1 + \frac{1}{2}\mathrm{B}_1 + 2\mathrm{C}_0\right)\cos\theta + \left(\frac{1}{2}\mathrm{B}_1 + \mathrm{B}_2\theta\right)\cos 3\theta\right.$$

$$\left. + \left(-2\mathrm{B}_2\theta^2 + (\mathrm{C}_2 - 2\mathrm{B}_1 + 2\mathrm{A}_1)\theta + 4\mathrm{A}_0 + \frac{1}{2}\mathrm{C}_1\right)\sin\theta + \left(\mathrm{C}_2\theta + \frac{1}{2}\mathrm{C}_1\right)\sin 3\theta\right\}$$

$$v_2^{\mathrm{A}}(\theta; \mathrm{Re}) = \mathrm{Re}\left\{\left(-2\mathrm{B}_2\theta^2 + (-2\mathrm{B}_1 + \mathrm{C}_2 - 2\mathrm{A}_1)\theta + \frac{1}{2}\mathrm{C}_1\right)\cos\theta\right.$$

$$\left. - \left(\frac{1}{2}\mathrm{C}_1 + \mathrm{C}_2\theta\right)\cos 3\theta + \left(-2\mathrm{C}_2\theta^2 - (\mathrm{B}_2 + 2\mathrm{C}_1)\theta + \mathrm{A}_1 - 2\mathrm{C}_0 - \frac{1}{2}\mathrm{B}_1\right)\sin\theta + \left(\frac{1}{2}\mathrm{B}_1 + \mathrm{B}_2\theta\right)\sin 3\theta\right\}$$

$$p_2^{\mathrm{A}} = \pi^2(8 - \pi^2)/(64\alpha^2)$$

$$\omega_2^{\mathrm{A}}(\theta; \mathrm{Re}) = 2\mathrm{Re}\{-(4\mathrm{C}_2\theta + 2\mathrm{C}_1 + \mathrm{B}_2)\cos 2\theta + (4\mathrm{B}_2\theta + 2\mathrm{B}_1 - \mathrm{C}_2)\sin 2\theta - 2\mathrm{A}_0 - 2\mathrm{A}_1\theta\}$$

where

$$\alpha = \pi^2/4 - 1, \qquad \mathrm{A}_0 = -\pi(\pi^4 + 14\pi^2 - 24)/(1024\alpha^2),$$

$$\mathrm{A}_1 = -\pi^2(\pi^2 + 8)/(256\alpha^2), \qquad \mathrm{B}_1 = -(\pi^2 + 12)/(128\alpha^2),$$

$$\mathrm{B}_2 = -\pi/(16\alpha^2), \qquad \mathrm{C}_0 = (\pi^4 + 10\pi^2 + 24)/(512\alpha^2),$$

$$\mathrm{C}_1 = \pi(\pi^2 + 6)/(64\alpha^2), \qquad \mathrm{C}_2 = (\pi^2 - 4)/(64\alpha^2).$$

At corner B (1, 1), the polar coordinates are defined by $x = 1 + r\cos\theta$, $y = 1 + r\sin\theta$, with $\theta \in [\pi, 3\pi/2]$; the singular solution has the following expression:

$$\Psi^{\mathrm{B}} = r f_1^{\mathrm{B}}(\theta) + r^2 f_2^{\mathrm{B}}(\theta; \mathrm{Re}),$$

$$u^{\mathrm{B}} = u_1^{\mathrm{B}}(\theta) + r u_2^{\mathrm{B}}(\theta; \mathrm{Re}),$$

$$v^{\mathrm{B}} = v_1^{\mathrm{B}}(\theta) + r v_2^{\mathrm{B}}(\theta; \mathrm{Re}),$$

$$p^{\mathrm{B}} = r^{-1} p_1^{\mathrm{B}}(\theta; \mathrm{Re}) + p_2^{\mathrm{B}} \ln r,$$

$$\omega^{\mathrm{B}} = r^{-1}\omega_1^{\mathrm{B}}(\theta) + \omega_2^{\mathrm{B}}(\theta; \mathrm{Re}),$$

with

$$f_1^{\mathrm{B}}(\theta) = f_1^{\mathrm{A}}(\pi - \theta), \qquad f_2^{\mathrm{B}}(\theta; \mathrm{Re}) = -f_2^{\mathrm{A}}(\pi - \theta; \mathrm{Re}),$$

$$u_1^{\mathrm{B}}(\theta) = u_1^{\mathrm{A}}(\pi - \theta), \qquad u_2^{\mathrm{B}}(\theta; \mathrm{Re}) = -u_2^{\mathrm{A}}(\pi - \theta; \mathrm{Re}),$$

$$v_1^{\mathrm{B}}(\theta) = -v_1^{\mathrm{A}}(\pi - \theta), \qquad v_2^{\mathrm{B}}(\theta; \mathrm{Re}) = v_2^{\mathrm{A}}(\pi - \theta; \mathrm{Re}),$$

$$p_1^{\mathrm{B}}(\theta; \mathrm{Re}) = -p_1^{\mathrm{A}}(\pi - \theta; \mathrm{Re}), \qquad p_2^{\mathrm{B}} = p_2^{\mathrm{A}},$$

$$\omega_1^{\mathrm{B}}(\theta) = \omega_1^{\mathrm{A}}(\pi - \theta), \qquad \omega_2^{\mathrm{B}}(\theta; \mathrm{Re}) = -\omega_2^{\mathrm{A}}(\pi - \theta; \mathrm{Re}).$$